nanomaterials

MDPI

Article

Photocatalysts Based on Graphite-like Carbon Nitride with a Low Content of Rhodium and Palladium for Hydrogen Production under Visible Light

Angelina V. Zhurenok [1], Danila B. Vasichenko [1,2], Semen N. Berdyugin [2], Evgeny Yu. Gerasimov [1], Andrey A. Saraev [1], Svetlana V. Cherepanova [1] and Ekaterina A. Kozlova [1,*]

[1] Federal Research Center, Boreskov Institute of Catalysis SB RAS, Lavrentieva Ave. 5, Novosibirsk 630090, Russia; angelinazhurenok@gmail.com (A.V.Z.); vasilchenko@niic.nsc.ru (D.B.V.); gerasimov@catalysis.ru (E.Y.G.); asaraev@catalysis.ru (A.A.S.); svch@catalysis.ru (S.V.C.)

[2] Nikolaev Institute of Inorganic Chemistry, Siberian Branch of the Russian Academy of Science, Novosibirsk 630090, Russia; berdyugin@niic.nsc.ru

* Correspondence: kozlova@catalysis.ru

Abstract: In this study, we proposed photocatalysts based on graphite-like carbon nitride with a low content (0.01–0.5 wt.%) of noble metals (Pd, Rh) for hydrogen evolution under visible light irradiation. As precursors of rhodium and palladium, labile aqua and nitrato complexes $[Rh_2(H_2O)_8(\mu\text{-}OH)_2](NO_3)_4 \cdot 4H_2O$ and $(Et_4N)_2[Pd(NO_3)_4]$, respectively, were proposed. To obtain metallic particles, reduction was carried out in H_2 at 400 °C. The synthesized photocatalysts were studied using X-ray diffraction, X-ray photoelectron spectroscopy, UV–Vis diffuse reflectance spectroscopy and high-resolution transmission electron microscopy. The activity of the photocatalysts was tested in the hydrogen evolution from aqueous and aqueous alkaline solutions of TEOA under visible light with a wavelength of 428 nm. It was shown that the activity for the 0.01–0.5% $Rh/g\text{-}C_3N_4$ series is higher than in the case of the 0.01–0.5% $Pd/g\text{-}C_3N_4$ photocatalysts. The 0.5% $Rh/g\text{-}C_3N_4$ sample showed the highest activity per gram of catalyst, equal to 3.9 mmol g_{cat}^{-1} h^{-1}, whereas the most efficient use of the metal particles was found over the 0.1% $Rh/g\text{-}C_3N_4$ photocatalyst, with the activity of 2.4 mol per gram of Rh per hour. The data obtained are of interest and can serve for further research in the field of photocatalytic hydrogen evolution using noble metals as cocatalysts.

Keywords: photocatalysis; hydrogen evolution; $g\text{-}C_3N_4$; noble metals; rhodium; palladium

Citation: Zhurenok, A.V.; Vasichenko, D.B.; Berdyugin, S.N.; Gerasimov, E.Y.; Saraev, A.A.; Cherepanova, S.V.; Kozlova, E.A. Photocatalysts Based on Graphite-like Carbon Nitride with a Low Content of Rhodium and Palladium for Hydrogen Production under Visible Light. *Nanomaterials* **2023**, *13*, 2176. https://doi.org/10.3390/nano13152176

Academic Editors: Jose L. Hueso, Ewa Kowalska and Zhishun Wei

Received: 1 July 2023
Revised: 19 July 2023
Accepted: 24 July 2023
Published: 26 July 2023

1. Introduction

Due to the growth of economic and environmental problems associated with the use of fossil fuels [1,2], the demand for a transition to alternative energy is growing [3]. Particular attention should be paid to hydrogen as a replacement for traditional energy sources [4]. Hydrogen is an environmentally friendly fuel and does not emit toxic compounds during combustion [5]. One of the most well-known processes for producing hydrogen used in industry is steam reforming of natural gas [6]. Despite the efficiency of hydrogen production of this method, steam reforming is not an environmentally friendly process, since it is energy-consuming, carried out at high temperatures and pressures and does not exclude CO_2 emissions [7]. In this regard, photocatalytic hydrogen production is of particular interest [8,9]. In the 1970s, photocatalytic hydrogen production was first discovered by Fujishima and Honda by water splitting on semiconductor photocatalysts under light irradiation [10]. Solar energy is universal, and its reserves are unlimited [11], while photocatalytic hydrogen production is a process occurring under environmental conditions [12–14]. Thus, photocatalytic hydrogen production can be an effective solution for converting solar energy into hydrogen energy [8].

The main factor hindering the practical use of photocatalytic processes is the lack of efficient and at the same time stable heterogeneous photocatalysts operating under the

action of visible light, which makes up about 43% of the solar spectrum [10]. Recently, the graphitic carbon nitride g-C_3N_4 has attracted more attention from researchers [15]. This material has the properties of a semiconductor with a band gap of 2.7 eV and positions of the valence and conduction bands suitable for the photocatalytic water splitting [16]. One of the common methods for increasing the activity of g-C_3N_4, as well as other semiconductor photocatalysts, is the deposition of metal co-catalysts on the surface of semiconductors [17,18], which leads to the spatial separation of electron–hole pairs. Traditionally, different metals, including noble metals, like Fe, Mn, Zn, Ni, Ag, Au, Cu and Pt, are used as co-catalysts [19,20].

In general, all platinum group metals can act as cocatalysts for photocatalytic hydrogen evolution [3]. However, for g-C_3N_4, among noble metals, platinum is usually deposited to the surface as a cocatalyst [21]. It is believed that platinum is the most effective co-catalyst for the formation of hydrogen; this metal forms the highest Schottky barrier at the metal–semiconductor interface, as it has the highest work function relative to other metals [8]. At the same time, it would be interesting to compare the deposition of other precious metals from the platinum group (especially Rh and Pd), since both experimental and theoretical results [22–25] presented for the HER suggest that these noble metals are located at the top of the corresponding volcano plot, and, therefore, according to the Sabatier principle they should provide near-optimal activity for hydrogen production. Also, in view of the high volatility of noble metals prices, it seems pragmatic to have information on their substitutability in catalysis. The literature describes only a few works on the photocatalytic production of hydrogen over Rh/g-C_3N_4 [26] and Pd/g-C_3N_4 [27], respectively. However, Rh- and Pd-supported g-C_3N_4-based catalysts have previously been shown to perform well in ammonia borane hydrolysis [28–30] and various photocatalytic oxidation processes [31–33].

In our previous research on the synthesis of platinized TiO_2 and g-C_3N_4 for hydrogen production, the deposition of platinum by means of sorption of $(Bu_4N)_2[Pt(NO_3)_6]$ labile complex followed by reduction in a stream of hydrogen allows one to obtain very active Pt/TiO_2 and Pt/g-C_3N_4 photocatalysts. This approach has been proven to obtain highly dispersed states of noble metals (<1 nm), which are characterized by strong interaction with the support, which makes it possible to achieve high specific photocatalytic activity in target processes at a low metal content (up to 0.1 wt%) [34–36]. In this research, we aimed at the synthesis and investigation of photocatalysts based on graphitic carbon nitride with a low (0.01–0.5 wt%) content of noble metals (Pd, Rh) for hydrogen production under visible light. By analogy with platinized photocatalysts, highly labile complexes $[Rh_2(H_2O)_8(\mu\text{-}OH)_2](NO_3)_4 \cdot 4H_2O$ and $(Et_4N)_2[Pd(NO_3)_4]$ were used as precursors of rhodium and palladium, respectively; reduction in H_2 at 400 °C was used to obtain metallic particles. The photocatalysts were tested in the photocatalytic production of hydrogen from aqueous and alkaline solutions of triethanolamine. Regularities were found for the activity and stability of Rh/g-C_3N_4 and Pd/g-C_3N_4 photocatalysts depending on the mass fraction of metals and the basicity of the medium.

2. Materials and Methods

2.1. Reagents

The following reagents were used: melamine (Aldrich, 98%, Burlington, MA, USA), cyanuric acid (Aldrich, 98%, USA), acetone (Ekos-1, 98%, Staraya Kupavna, Russia), $RhCl_3$ (Krastsvetmet, 38.67% of Rh, Krasnoyarsk, Russia), pure Pd powder acid (Krastsvetmet, 99.99%, Krasnoyarsk, Russia).

2.2. g-C_3N_4 Synthesis

The proposed method for the synthesis of g-C_3N_4 consists of the thermolysis of the supramolecular melamine–cyanuric acid adduct [35]. Melamine (40.5 g, Aldrich, 98%) and cyanuric acid (41.5 g, Aldrich, 98%) were suspended in distilled water (300 mL) and heated at 90 °C for 12 h under continuous stirring. The suspension then was cooled, and a white

solid was filtered off, which was then washed and dried in vacuum. The resulting material was placed in a muffle and kept at the temperature 550 °C for 1 h; the heating rate was 1 °C/min. The resulting light-yellow sample of g-C_3N_4 was ground in a mortar.

2.3. Rh and Pd Deposition

$[Rh_2(H_2O)_8(\mu\text{-}OH)_2](NO_3)_4 \cdot 4H_2O$ (prepared from K_3RhCl_6 [37]) was dissolved in acetone + ethanol (3%) to obtain a solution with [Rh] of 0.568 mM (Rh solution). Also, $(Et_4N)_2[Pd(NO_3)_4]$ (prepared from metallic palladium [38]) was dissolved in acetone to obtain a solution with [Pd] of 2.76 mM (Pd solution). An appropriate aliquot of Rh solution (11 mL for 0.5%, 2.2 mL for 0.1%, 1.1 mL for 0.05%, 0.22 mL for 0.01%), or Pd solution (4.8 mL for 0.5%, 0.96 mL for 0.1%, 0.48 mL for 0.05%, 0.096 mL for 0.01%), was added into a suspension of g-C_3N_4 (250 mg) in 1.5 mL of acetone. The resulting suspensions were thoroughly mixed for one (Pd) or five (Rh) days at room temperature until the mother liquor become colorless. The powder was separated by filtration, washed with acetone and dried in an air flow. The dried powders were heated in a stream of hydrogen at 400 °C for 1 h yielding the X%M/g-C_3N_4 (M = Rh or Pd) catalysts, where X = 0.5, 0.1, 0.05 or 0.01 and designates the percentage of corresponding metal (weight percent). For comparison, the deposition of 0.5% of Pd and Rh from solutions of $[Pd(NH_3)_4(NO_3)_2]$ and $RhCl_3$ was carried out using the same technique.

2.4. Photocatalyst Characterization

The photocatalysts were characterized by X-ray diffraction (XRD), X-ray photoelectron spectroscopy (XPS), UV–Vis spectroscopy and high-resolution transmission electron microscopy (HRTEM) techniques. XRD investigations was performed with a D8 Advance powder diffractometer (Bruker, Germany) using CuKα radiation. XRD patterns were recorded in the 2θ range from 20° to 80°. The mean sizes of crystallites were estimated from the full width at half maximum of the corresponding peaks using the Scherrer formula as follows:

$$d = \frac{K \times \lambda}{\beta cos\theta} \quad (1)$$

where d—average size of coherent scattering crystallites (nm), K—Scherrer constant, λ—X-ray wavelength (nm), β—width of reflection at half height (2θ units), θ—diffraction angle.

XPS studies were carried out on a SPECS Surface Nano Analysis GmbH photoelectron spectrometer (Berlin, Germany) with monochromatic AlKα radiation. Diffuse reflectance spectra were recorded on a UV-2501 PC spectrophotometer (Shimadzu, Japan) equipped with an ISR-240A diffuse reflectance cell. The structure of the photocatalysts was studied by HRTEM using a ThemisZ electron microscope (Thermo Fisher Scientific, Waltham, MA, USA) operated at an accelerating voltage of 200 kV.

Elemental analysis was carried out for several samples with the ICP-AES technique with the use of an iCAP-6500 high-resolution spectrometer (Thermo Scientific, Waltham, MA, USA, (ICP-AES)) with a cyclone-type spray chamber and a SeaSpray nebulizer. The actual content of metals was in good agreement with calculated values (Table S1).

2.5. Photocatalytic Activity

The activity of the photocatalyst was investigated in a batch reactor. The reaction suspension containing 50 mg of a photocatalyst and 100 mL of an aqueous or aqueous alkaline (C_0(NaOH (Aldrich, 98%)) 10 vol.% triethanolamine (TEOA, Reachim, 98%) solution was purged with argon for 30 min to remove oxygen before the start of the photocatalytic reaction. Then, the suspension was irradiated using an LED radiation source (λ = 428 nm, 56 mW/cm^2). The area of the quartz window of the reactor was 22.5 cm^2. The amount of hydrogen evolved was measured using a gas chromatograph (Khromos, Russia); the reaction duration was 90 min.

The apparent quantum efficiency (AQE) was calculated as follows:

$$AQE = \frac{2 \times W_0}{N_{ph}} \times 100\% \quad (2)$$

where W_0—reaction rate (μmol min^{-1}), N_{ph}—photon flux constituting 283 μEinstein min^{-1}. The number of electrons (2) involved in the hydrogen formation reaction was taken into account in the apparent quantum efficiency calculation.

3. Results

3.1. Photocatalyst Characterization

3.1.1. X-ray Diffraction

In order to characterize the crystalline phase of the Pd/g-C_3N_4 and Rh/g-C_3N_4 samples, XRD patterns of the synthesized photocatalysts were obtained (Figure 1). Figure 1 shows that there are two main peaks in the XRD patterns, located at 13 and 27°; these peaks can be attributed to g-C_3N_4 [16]. The peak located at 13° corresponds to the reflection from the (210) plane and is due to the distance between the heptazine (tri-s-triazine) units in the 2D g-C_3N_4 layer, and the diffraction peak (2θ~27°) belongs to the (002) plane and determines the distance between the 2D layers of g-C_3N_4 [35,39]. It can be seen that the characteristic g-C_3N_4 peak at 27° becomes broader and weaker with the increase in Pd and Rh content (Figure 1). For the sample 0.5% Pd/g-C_3N_4, a characteristic peak at 40.1° appears, which belongs to the (111) diffraction plane of metallic Pd (Figure 1b). For the rest of the rhodium- and palladium-containing samples, no metal peaks were found, probably due to low mass fraction of Rh and Pd.

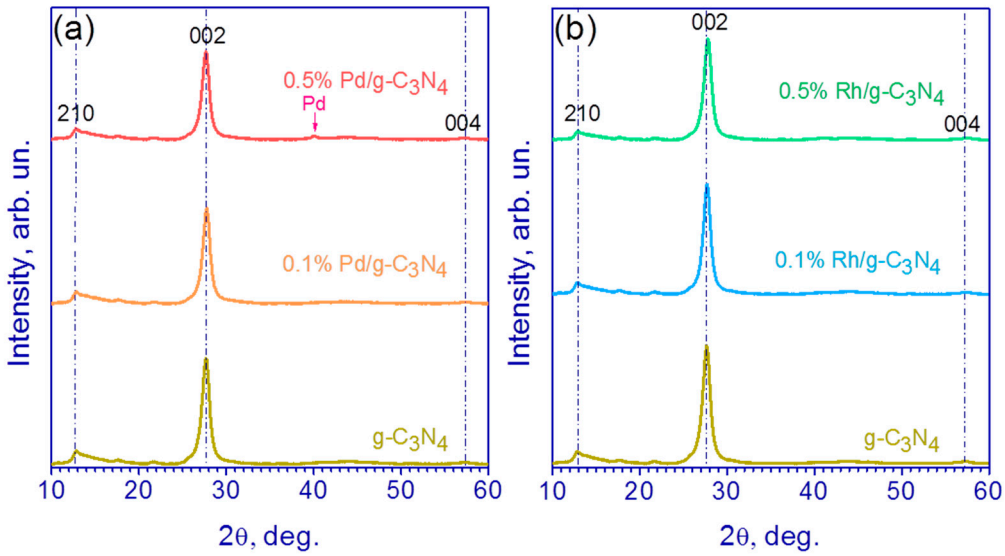

Figure 1. XRD patterns of pristine g-C_3N_4, (**a**) Pd (0.1 and 0.5 wt%)/g-C_3N_4 and (**b**) Rh (0.1 and 0.5 wt%)/g-C_3N_4.

The interlayer distance d_{002} for the all samples was ca. 3.22 Å, which is in good agreement with the data obtained for g-C_3N_4 [39]. The average crystallite size in the plane of the layer was 9.5–9.6 nm, and the average crystallite size in the direction perpendicular to the layer was 9.3–9.8 nm.

3.1.2. UV–Vis Spectroscopy

The optical properties of synthesized photocatalysts were investigated using UV–Vis spectroscopy (Figure 2). One can see that the absorption edge for all samples is ca. 400 nm (Figure 2a,c). Also, the deposition of noble metals promotes the adsorption of visible light in the range 400–800 nm. Figure 2b,d show the data transformation for pristine g-C_3N_4, Pd (0.1 and 0.5 wt.%)/g-C_3N_4 and Rh (0.1 and 0.5 wt.%)/g-C_3N_4 photocatalysts in Tauc's

coordinates for indirect semiconductors. It was shown that the deposition of metals has almost no effect on the band gap energy, which is in the range of 2.77–2.83 eV for all the samples.

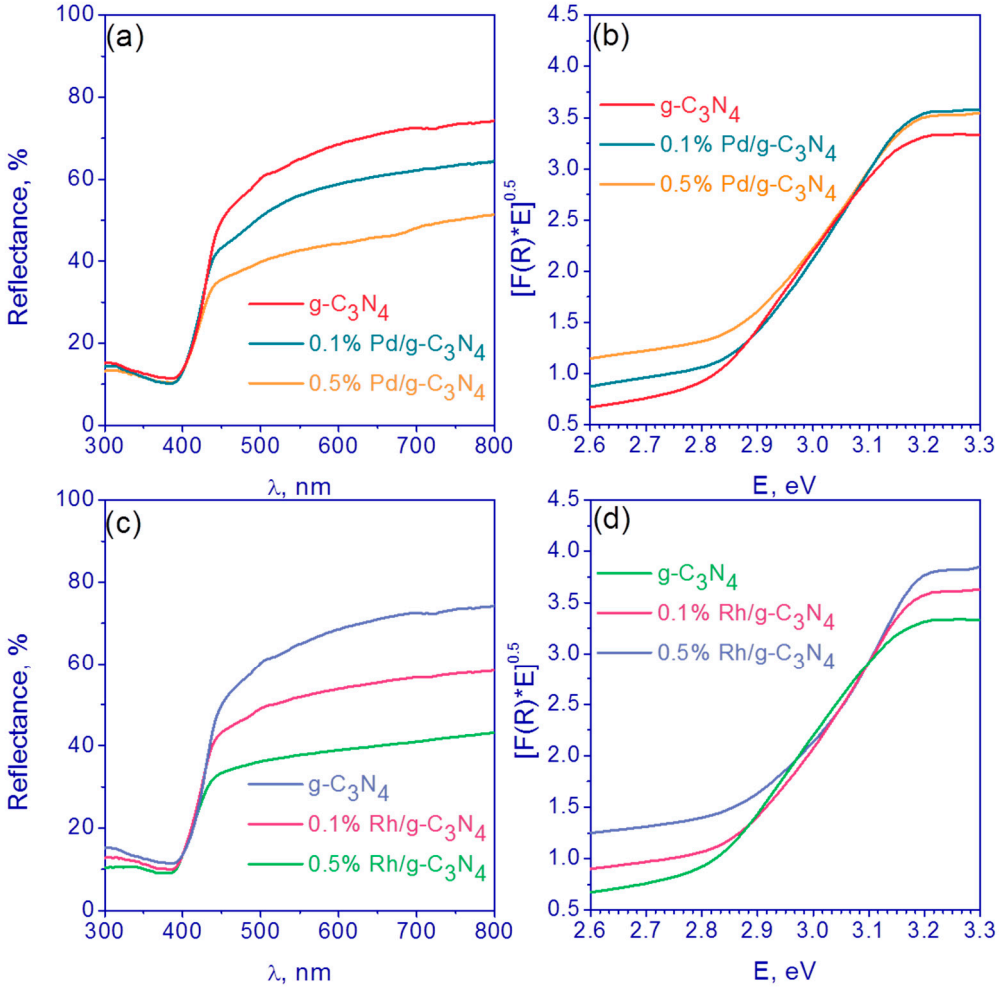

Figure 2. (**a**,**c**) Diffuse reflectance spectra and (**b**,**d**) Tauc plots of (**a**,**b**) pristine g-C_3N_4, Pd (0.1 and 0.5 wt.%)/g-C_3N_4 and (**c**,**d**) Rh (0.1 and 0.5 wt.%)/g-C_3N_4.

3.1.3. HR TEM Method

High-resolution TEM images show the morphology of 0.5% Pd/g-C_3N_4 (Figure 3) and 0.5% Rh/g-C_3N_4 (Figure 4) photocatalysts and corresponding particle size distributions. Fourier transform of TEM images (Figure S1) reveals the interplanar distance of 3.3 Å, which is in good agreement with the interplanar distance determined from the XRD patterns (Figure 1) and with the previously published data [35,39,40]. One can see that both Pd and Rh particles have spherical shape. The average metal particles size was 3.1 ± 2.1 nm for Pd (Figure 3d) and 2.5 ± 1.2 nm for Rh (Figure 4d), respectively. The particle size distribution of both Pd and Rh includes particles ranging in size from 1 to 7 nm (Figures 3d and 4d). In addition, it should be noted that palladium forms large clusters 20–30 nm in size, while rhodium is more evenly distributed over the surface of g-C_3N_4. We can assume that rhodium complexes are adsorbed on the g-C_3N_4 surface more uniformly, which is associated with the preferred structure of the complex $Rh_2(H_2O)_8(\mu\text{-}OH)_2](NO_3)_4{\cdot}4H_2O$ compared to $(Et_4N)_2[Pd(NO_3)_4$.

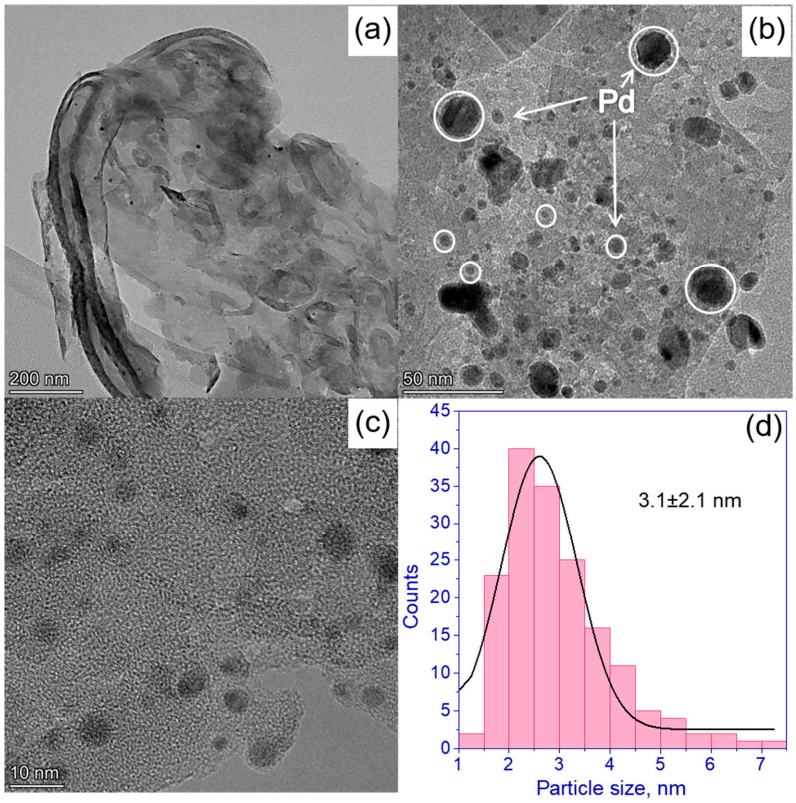

Figure 3. (**a**–**c**) HRTEM images of 0.5% Pd/g-C_3N_4 photocatalyst; (**d**) Pd particle size distribution calculated based on HRTEM data.

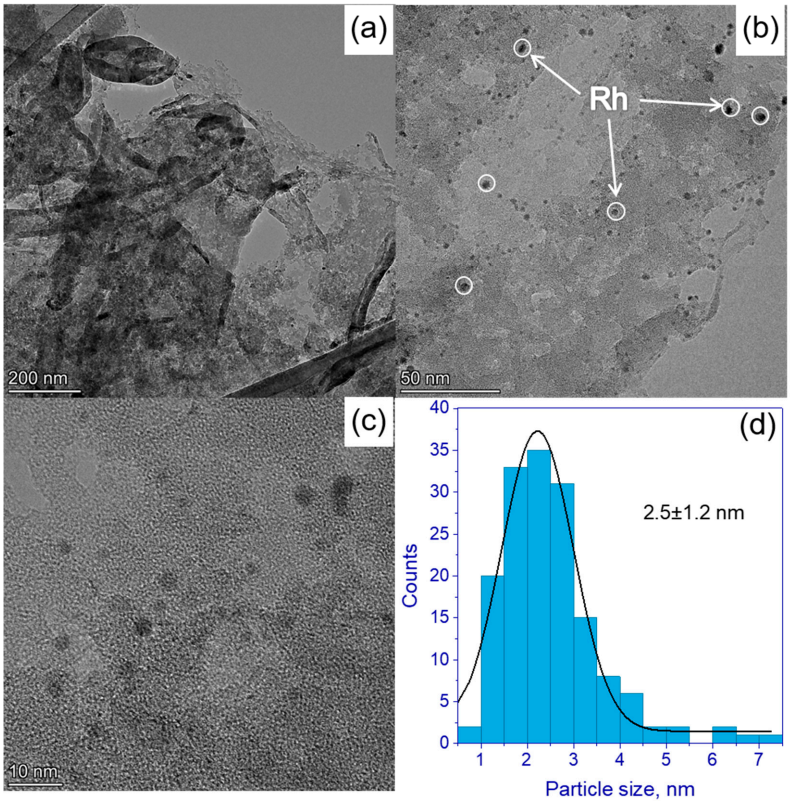

Figure 4. (**a**–**c**) HRTEM images of 0.5% Rh/g-C_3N_4; (**d**) Rh particle size distribution calculated based on HRTEM data.

HRTEM images were also used to confirm the presence of Pd and Rh in the synthesized photocatalysts (Figure S2). The observed distances for 0.5% Rh/g-C_3N_4 were equal to 2.19 and 1.91–1.92 Å, corresponding to Rh planes (111) and (200), respectively (PDF No. 5-685). A similar situation is observed for the 0.5% Pd/g-C_3N_4 photocatalyst. The interplane distances were equal to 2.28 and 2.09 Å, respectively, corresponding to the Pd planes (111) and (200) (PDF No. 46-1043).

3.1.4. XPS Method

The study of the chemical composition of the samples was carried out with the XPS technique. The XPS spectra of the catalysts revealed peaks corresponding to Pd, Rh, N, C and O. Figure 5a,b shows the C1s and N1s spectra of pristine g-C_3N_4. The C1s spectrum is well described by two peaks with binding energies of 284.9 and 288.1 eV. The first peak is characteristic of carbon-containing impurities present on the surface of the objects under study (often used to calibrate the binding energy scale). The second peak is characteristic of C1s g-C_3N_4 and corresponds to carbon forming bonds with nitrogen atoms in the g-C_3N_4 structure [41,42]. In the case of the N1s spectrum, four peaks are observed with binding energies of 398.6, 400.0, 401.0 and 404.5 eV. According to the literature data, the first peak refers to nitrogen atoms forming a C-N=C bond, the second one to N-$(C)_3$ bonds with three carbon atoms, the third one to the N-H terminal groups and the fourth peak corresponds to an excited π bond [41].

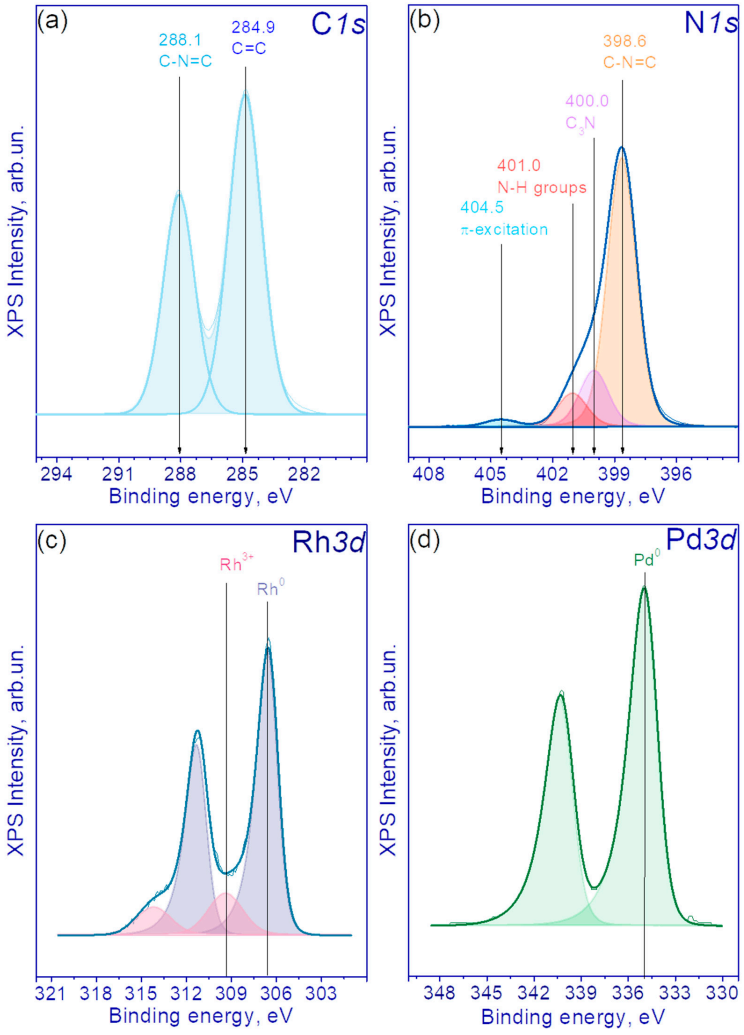

Figure 5. (**a**) The C1s and (**b**) N1s XPS spectra of pristine g-C_3N_4; (**c**) Rh3d spectra of 0.5%Rh/g-C_3N_4 and (**d**) Pd3d spectra of 0.5%Pd/g-C_3N_4.

Figure 5c shows the Rh3d spectra for the photocatalyst 0.5%Rh/g-C_3N_4. The Rh3d spectrum is described by one asymmetric $Rh4f_{7/2}$–$Rh4f_{7/2}$ doublet with a $Rh3d_{5/2}$ binding energy of 306.5 eV and one symmetrical $Rh4f_{7/2}$–$Rh4f_{7/2}$ doublet with a $Rh3d_{5/2}$ binding energy of 309.4 eV. In the literature, for metallic Rh, the binding energy of $Rh4f_{7/2}$ is equal to 306.7–307.5 eV, and for Rh_2O_3 it lies in the range of 309.4–310.2 eV [28]. Thus, the doublet in the region of high binding energies refers to rhodium in the Rh^{3+} state, and the narrow asymmetric doublet in the lower binding energies region can be attributed to rhodium in the metallic state Rh^0. According to the analysis, the proportion of Rh in the metallic state is 75%, and rhodium in the Rh^{3+} state is 25%, respectively. Figure 5d shows the Pd3d spectra of the 0.5% Pd/g-C_3N_4 photocatalyst. The Pd3d spectrum is well described by the $Pd3d_{5/2}$-$Pd3d_{3/2}$ doublet with $Pd3d_{5/2}$ binding energy of 335.0 eV. For palladium in the metallic state, the $Pd3d_{5/2}$ binding energy is 335.0–335.2 eV [32], and for PdO it is 336.6–337.7 eV [32,43]. Thus, in 0.5% Pd/g-C_3N_4 catalyst, Pd exists completely in the metallic state.

The atomic percentages of the surface for the samples 0.5% Rh/g-C_3N_4 and 0.5% Pd/g-C_3N_4 are shown in Table S2. It can be seen that the surface content of rhodium is much higher than in the case of palladium at the same weight content. The presented data on the surface content of rhodium and palladium once again confirm that in the case of the first metal, the deposition occurs with the formation of smaller particles with a good coverage of the g-C_3N_4 surface.

In general, from the characterization of photocatalysts, it can be concluded that 0.01–0.5% Pd/g-C_3N_4 and 0.01–0.5% Rh/g-C_3N_4 samples were obtained. In the case of the reduction of palladium from $(Et_4N)_2[Pd(NO_3)_4]$ complex, it was possible to achieve a completely metallic state, whereas in the case of the use of $[Rh_2(H_2O)_8(\mu\text{-}OH)_2](NO_3)_4{\cdot}4H_2O$ as a rhodium precursor, complete reduction of the metal was not achieved.

3.2. Photocatalyst Characterization

The activity of all synthesized samples 0.01–0.5% Pd/g-C_3N_4 and 0.01–0.5% Rh/g-C_3N_4, as well as the activity of pristine g-C_3N_4 and Pd- and Rh-containing samples before the reduction in hydrogen (with adsorbed complexes of palladium or rhodium after drying), was studied in the photocatalytic production of hydrogen in aqueous and aqueous alkaline solutions of TEOA. TEOA was chosen as a sacrificial agent as it helps to reduce photocorrosion of g-C_3N_4 because the amino groups of TEOA effectively bind to the surface of g-C_3N_4 [44,45]. Alkaline solution was used to facilitate proton abstraction during TEOA oxidation and to prevent charge recombination on the catalyst surface [46]. The photocatalytic activity was studied with the use of LED with a maximum emission at a wavelength of 428 nm as a light source (Figure 6a). Previously, it was shown that when using a diode with a maximum radiation in this region, the highest AQE was observed [35]. Note that over pristine g-C_3N_4, the rate was equal to zero both under neutral and alkali conditions. Figure 6b shows the kinetics of hydrogen formation for 0.1% Pd/g-C_3N_4 and 0.1% Rh/g-C_3N_4 samples without heat treatment and with H_2 reduction at 400 °C.

One can see that the activity of photocatalysts with adsorbed complexes of rhodium and palladium is an order of magnitude lower than after the reduction of the corresponding complexes with H_2 at 400 °C. As shown earlier for platinized photocatalysts, treatment with H_2 at 400 °C is a necessary step for the formation of a metal cocatalyst for hydrogen evolution on the surface of g-C_3N_4 [35]. The next step in the study was to vary the mass fraction of metals from 0.01 to 0.5%. As was described before, $[Rh_2(H_2O)_8(\mu\text{-}OH)_2](NO_3)_4{\cdot}4H_2O$ and $(Et_4N)_2[Pd(NO_3)_4]$ were used as precursors of rhodium and palladium, respectively; reduction in H_2 at 400 °C was used to obtain metallic particles for all samples. The data on activities of all the samples per 1 g of catalyst and per 1 g of noble metal are represented in Table 1.

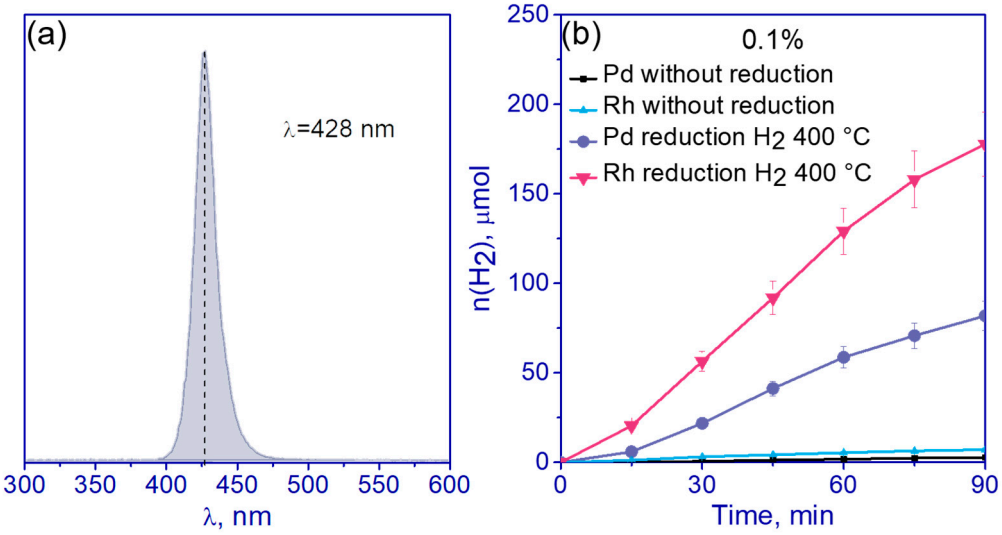

Figure 6. (**a**) Emission spectrum of 428 nm LED used as a light source; (**b**) the kinetic curves of photocatalytic hydrogen evolution over 0.1% Rh/g-C_3N_4 and 0.1% Pd/g-C_3N_4 without H_2 reduction and with H_2 reduction at 400 °C. Conditions: C(cat) = 0.5 g/L, 10 vol.% TEOA, C_0(NaOH) = 0.1 M.

Table 1. Photocatalytic properties of the synthesized samples and comparison with the literature data.

No.	Photocatalyst	Metal Weight Content, %	Catalytic Activity, μmol g_{cat}^{-1} h^{-1}	Catalytic Activity, mol g_{Metal}^{-1} h^{-1}	AQY, %	Ref.
1	g-C_3N_4	-	<1	0	0	
			Pd/g-C_3N_4			
2	Pd/g-C_3N_4	0.01	96	1.0	<0.1	This study
3		0.05	620	1.2	0.4	
4		0.1	1080	1.1	0.7	
5		0.5	3100	0.6	1.8	
6	Pd/g-C_3N_4 (from $[Pd(NH_3)_4(NO_3)_2]$)	0.5	1730	0.3	1.0	
7	Pd/g-C_3N_4 (from $PdCl_2$)	0.5	3300	0.7	-	[27] *
8		0.5	7600	1.5	2.4 (400 nm)	
			Rh/g-C_3N_4			
9	Rh/g-C_3N_4	0.01	88	0.9	<0.1	This study
10		0.05	732	1.5	0.4	
11		0.1	2400	2.4	1.4	
12		0.5	3900	0.8	2.3	
13	Rh/g-C_3N_4 (from $RhCl_3$)	0.5	610	0.1	0.4	
14	Rh/g-C_3N_4 (from $RhCl_3$)	0.25	14.9	0.006	-	[26] **
15		0.23	13.3	0.006		
16	Rh/g-C_3N_4 (from $Rh(acac)_3$	0.34	10.7	0.003		
17		0.27	3.8	0.001		
			Pt/g-C_3N_4			
18	$Pt_{0.1}$/g-C_3N_4	0.1	8520	8.5	5.0	[35] ***
19	$Pt_{0.5}$/g-C_3N_4	0.5	11,300	2.2	6.6	
20	$Pt_{0.1}$/g-C_3N_4	0.1	7560	7.6	4.4	[47] ***
21	$Pt_{0.5}$/g-C_3N_4	0.5	8520	1.7	5.0	

* Substrate—10 vol.% TEOA, λ = 400 nm. ** Substrate—10 vol.% methanol, Xe arc lamp with cut-off filter λ = 420 nm. *** Conditions are the same as for photocatalysts No. 1–6 and 7–10.

The photocatalytic activities vs. metal loading are shown in Figure 7. As can be seen, the catalytic activity increases with the increase in a metal content for both Pd and Rh (Figure 7a,c), and the highest catalytic activities were observed for 0.5% Rh/g-C_3N_4 and 0.5%Pd/g-C_3N_4 photocatalysts (Figure 7a,c). The activity of 0.5% Rh/g-C_3N_4

photocatalysts was equal to ca. 3.9 mmol H_2 per gram per hour and was about 25% higher than the activity of the photocatalyst 0.5% Pd/g-C_3N_4. Recalculation of activity per 1 g of metal showed that the maximum value and the most efficient use of the metal was observed for 0.1% Rh/g-C_3N_4 and was equal to 2.4 mol H_2 per gram of Rh per hour (Figure 7d). This parameter was already twice that of the photocatalyst 0.1% Pd/g-C_3N_4.

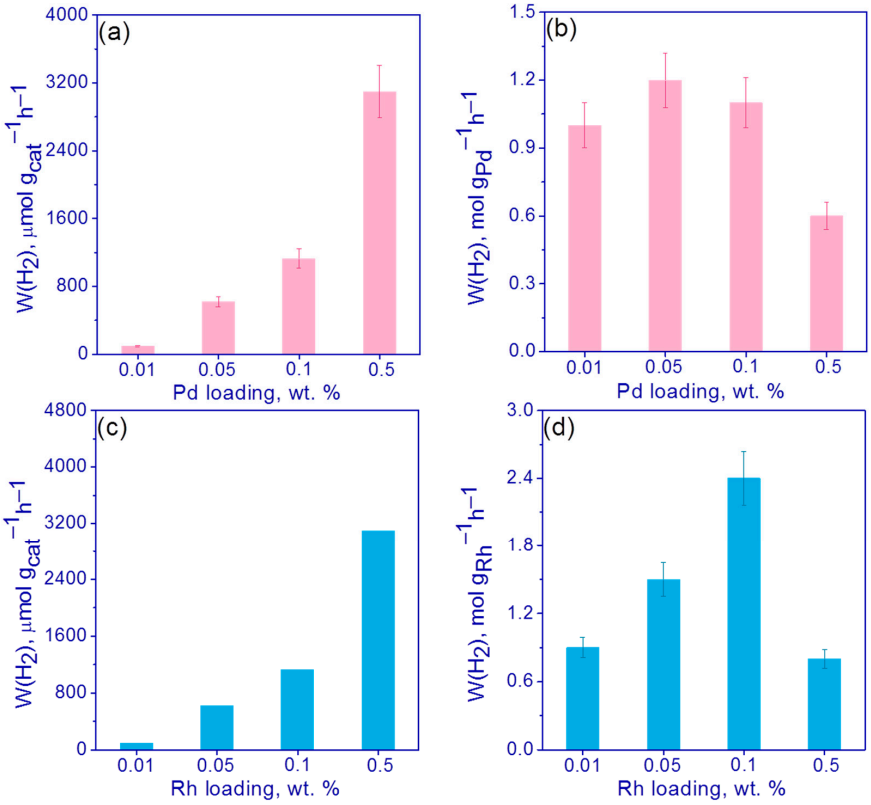

Figure 7. (**a**,**b**) Activity of 0.01–0.5% Pd/g-C_3N_4 and (**c**,**d**) 0.01–0.5% Rh/g-C_3N_4 photocatalysts in hydrogen evolution (**a**,**c**) per 1 g of catalyst and (**b**,**d**) per 1 g of metal. Conditions: C(cat) = 0.5 g/L, 10 vol.% TEOA, C_0(NaOH) = 0.1 M, 428 nm LED.

Thus, it can be concluded that in the case of supported rhodium for the Rh/g-C_3N_4 photocatalysts, the use of Rh nanoparticles in the formation of hydrogen is more efficient than in the case of supported palladium for the photocatalysts Pd/g-C_3N_4. This may be due to the fact that the palladium deposited on the surface of the carbon nitride has a larger particle size compared to rhodium (Figures 3 and 4). In addition, as can be seen from Figure 3b, palladium particles are collected into large aggregates, which can adversely affect the photocatalytic activity. The effect of metal nanoparticles—rhodium and palladium—as cocatalysts of hydrogen formation is likely similar. The deposition of metals leads to the separation of photogenerated charges due to the appearance of a Schottky barrier at the metal–semiconductor interface [8]. The main factor affecting the activity is most likely the formation of large agglomerates in the case of deposited rhodium. These large metal particles prevent the absorption of light by the semiconductor and can act as centers for the recombination of electron–hole pairs.

We compared numerical values obtained in this study with our previous results on platinized photocatalysts obtained with the $(Bu_4N)_2[Pt(NO_3)_6]$ labile complex as a platinum precursor [35,45] as well as with previously published data on Pd/g-C_3N_4 [27] and Rh/g-C_3N_4 [26] photocatalysts. It has been shown that with similar methods of synthesis with the deposition of noble metals from labile precursor complexes, the highest activity in the series of Pt, Rh and Pd metals is observed for platinum. Thus, for the photocatalyst 0.5% Rh/g-C_3N_4 under study, the activity per gram of catalyst was 4 mmol g^{-1} h^{-1}, and

for the photocatalyst 0.5% Pt/g-C_3N_4 [35] it was 11 mmol g^{-1} h^{-1}; the difference in the highest specific activity per gram of metal was also about 3 times higher for platinum photocatalysts (Table 1). Platinum is known as the most effective co-catalyst for the formation of hydrogen because Pt forms the highest Schottky barrier at the metal–semiconductor interface, due to the highest work function relative to other metals [8]. It is interesting to note that the activity of palladium photocatalysts Pd/g-C_3N_4 obtained using $(Et_4N)_2[Pd(NO_3)_4]$ complex as a precursor of palladium is approximately on the same level as for photocatalysts for which ordinary palladium chloride acted as a precursor [27]. At the same time, Table 1 shows that the activity of rhodium photocatalysts Rh/g-C_3N_4 obtained using $[Rh_2(H_2O)_8(\mu\text{-}OH)_2](NO_3)_4{\cdot}4H_2O$ complex as a precursor is orders of magnitude higher than the activity of photocatalysts Rh/g-C_3N_4 in which $RhCl_3$ or $Rh(acac)_3$ acted as a rhodium precursor [26]. In order to justify the choice of the precursor, the deposition of Pd and Rh (0.5 wt%) on the surface of g-C_3N_4 with the use of $[Pd(NH_3)_4(NO_3)_2]$ and $RhCl_3$ as precursors, respectively, was carried out. The activity in the photocatalytic hydrogen evolution was lower by ca. 2 and 6 times for 0.5% Pd/g-C_3N_4 and 0.5% Rh/g-C_3N_4 photocatalysts compared to similar samples synthesized with the use of $(Et_4N)_2[Pd(NO_3)_4]$ and $[Rh_2(H_2O)_8(\mu\text{-}OH)_2](NO_3)_4{\cdot}4H_2O$ precursors (Figure S3). Thus, the synthesis method proposed in this work for 0.01–0.5% Rh/g-C_3N_4 photocatalysts can be considered quite promising, especially considering the acceptable activity at low mass fractions of the metal.

Next, the stability of the most active photocatalysts, 0.5 wt.% Pd/g-C_3N_4 and 0.5 wt.% Rh/g-C_3N_4, was investigated in four runs in alkali (C_0(NaOH) = 0.1 M) suspensions of TEOA, each of which lasted 1.5 h. After every 1.5 h of the reaction cycle, the suspension was purged with argon for 30 min. Figure 8a,c shows the kinetic curves and Figure 8b,d shows H_2 evolution rates for the cyclic experiments.

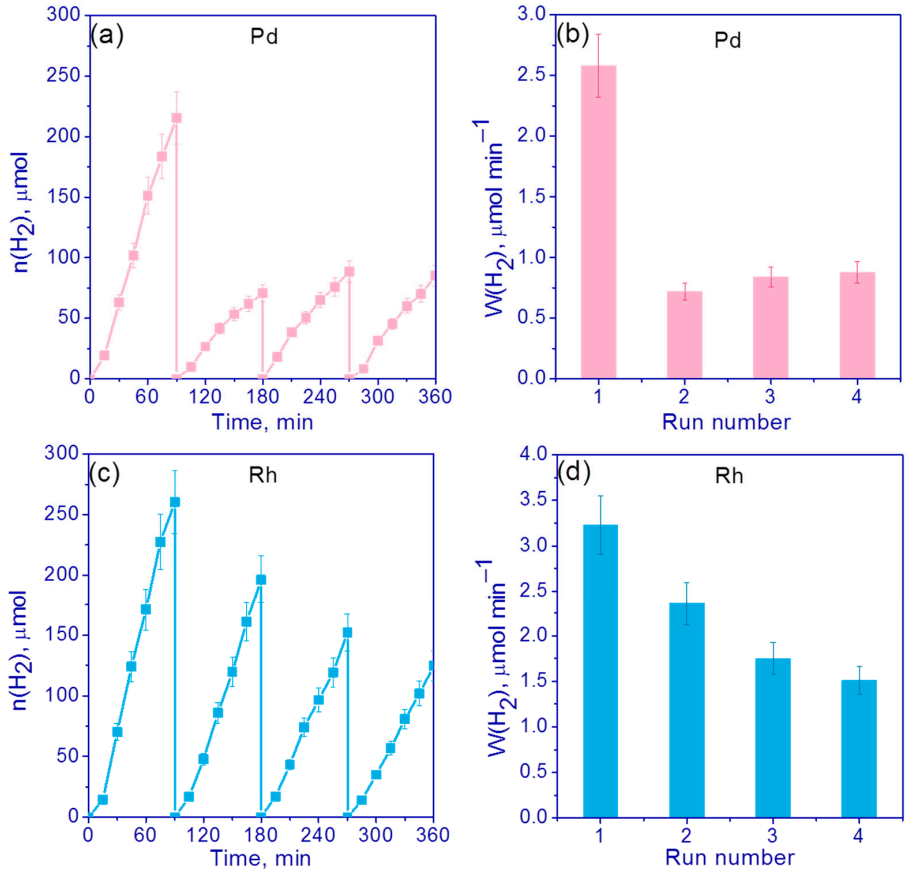

Figure 8. (**a**,**c**) The kinetic curves and (**b**,**d**) H_2 evolution rates for photocatalysts (**a**,**b**) 0.5% Pd/g-C_3N_4 and (**c**,**d**) 0.5% Rh/g-C_3N_4. Conditions: C(cat) = 0.5 g/L, 10 vol.% TEOA, C_0(NaOH) = 0.1 M, 428 nm LED.

In the case of a 0.5% Pd/g-C_3N_4 photocatalyst, the activity dropped sharply after the first run and then remained unchanged for three runs (Figure 8a,b). The drop in the activity was by approximately three times (Figure 8b). As can be seen, the deactivation of 0.5% Rh/g-C_3N_4 occurred gradually, and no sharp drop in activity is observed after the first cycle (Figure 8c,d). However, after the fourth cycle, the hydrogen evolution rate became 2 times lower compared to the first cycle (Figure 8d). Judging from the data of cyclic experiments, the decrease in activity in the case of photocatalysts with rhodium and palladium proceeded through different mechanisms. It can be assumed that the deactivation of the catalysts is most likely associated with the poisoning of active centers by TEOA oxidation products [35]. In order to reduce the influence of the resulting TEOA oxidation products, it was decided to study the stability of 0.5% Pd/g-C_3N_4 and 0.5% Rh/g-C_3N_4 under neutral conditions without addition of NaOH (Figure 9).

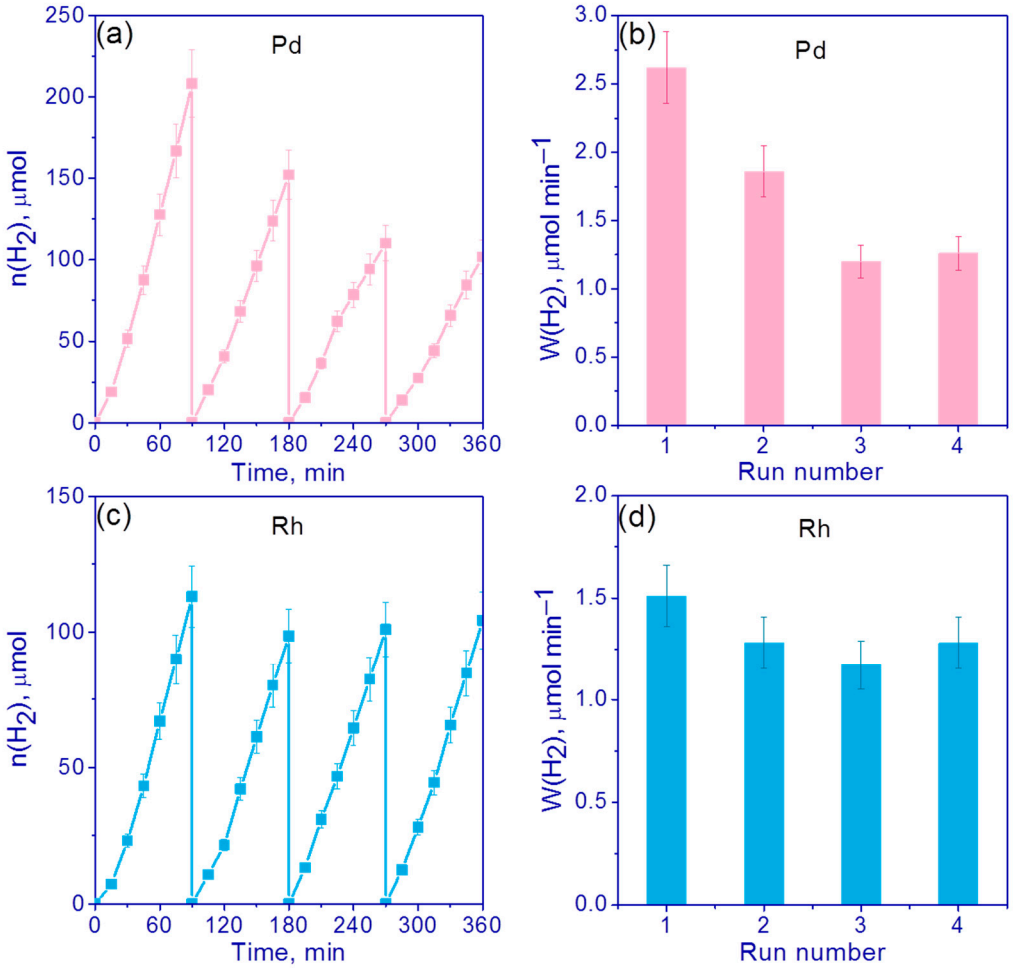

Figure 9. (**a**,**c**) The kinetic curves and (**b**,**d**) H_2 evolution rates for (**a**,**b**) 0.5% Pd/g-C_3N_4 and (**c**,**d**) 0.5% Rh/g-C_3N_4. Conditions: C(cat) = 0.5 g/L, 10 vol.% TEOA, 428 nm LED.

Figure 9c,d show that in the absence of NaOH, deactivation practically did not occur in the case of 0.5% Rh/g-C_3N_4 and amounted to only 15% (Figure 9c,d). However, in general, the activity was lower (Figure 9c,d) than in the experiments in alkaline media with addition of NaOH (Figure 8c,d). Thus, for the first run, the rate was 2 times lower compared to the experiments in the alkaline suspension of TEOA. In the case of 0.5% Pd/g-C_3N_4, the hydrogen evolution rate did not decrease compared to the experiments where NaOH was added into the reaction suspension; however, a twofold decrease in the rate after four runs was still observed (Figure 9a,b). We compared the surface content of elements before and after the photocatalytic tests for the samples 0.5% Pd/g-C_3N_4 and 0.5% Rh/g-C_3N_4 using

the XPS technique (Table S2). It was shown that for 0.5% Rh/g-C_3N_4 photocatalysts, after the hydrogen evolution both in alkaline media and without NaOH addition, all rhodium became metallic with zero oxidation state; for both cases, the surface content of the metal fell by 2 times but remained rather high. In the case of tests in a 0.1 M NaOH medium, significant surface carbonization was observed, which is probably the cause of deactivation. For the 0.5 % Pd/g-C_3N_4 photocatalyst, we observed the decrease in surface Pd content only in alkaline media; however, the deactivation was observed both in the cases of alkaline and neutral media (Figures 8 and 9).

In general, it should be noted that the deactivation mechanisms differ for the Rh/g-C_3N_4 and Pd/g-C_3N_4 photocatalysts, which is associated with different charge states of metals and their particle size distribution and requires further study.

4. Conclusions

In this research, a series of photocatalysts 0.01–0.5% Pd/g-C_3N_4 and 0.01–0.5% Rh/g-C_3N_4 was synthesized and characterized by a set of physicochemical methods. A distinctive feature of the synthesis was the use as precursors of such labile complexes as $[Rh_2(H_2O)_8(\mu\text{-}OH)_2](NO_3)_4{\cdot}4H_2O$ and $(Et_4N)_2[Pd(NO_3)_4]$ with further reduction in H_2 at 400° in order to obtain metallic particles of rhodium and palladium, respectively. It has been shown that in the case of the reduction of palladium from $(Et_4N)_2[Pd(NO_3)_4]$ complex, it is possible to achieve a completely metallic state, whereas in the case of the use of $[Rh_2(H_2O)_8(\mu\text{-}OH)_2](NO_3)_4{\cdot}4H_2O$, rhodium exists in the Rh^0 and Rh^{3+} states.

It was shown that the activity in the hydrogen evolution from aqueous solutions of TEOA under visible light for the 0.01–0.5% Rh/g-C_3N_4 series is higher than in the case of the 0.01–0.5% Pd/g-C_3N_4 photocatalysts. For the Rh/g-C_3N_4 photocatalysts, the use of Rh nanoparticles in the formation of hydrogen is likely more efficient than in the case of supported palladium for the photocatalysts Pd/g-C_3N_4 because palladium particles are collected into large aggregates, which can adversely affect the photocatalytic activity. The highest activity per gram of photocatalysts was possessed by the sample 0.5% Rh/g-C_3N_4 and was equal to ca. 3.9 mmol H_2 g^{-1} h^{-1}; the highest activity per gram of metal was possessed by 0.1% Rh/g-C_3N_4 and was equal to 2.4 mol H_2 $g_{Rh}{}^{-1}$ h^{-1}. It is interesting to note that the activity of the Rh/g-C_3N_4 photocatalysts obtained using $[Rh_2(H_2O)_8(\mu\text{-}OH)_2](NO_3)_4{\cdot}4H_2O$ complex as a precursor is orders of magnitude higher than the activity of photocatalysts Rh/g-C_3N_4 in which $RhCl_3$ or $Rh(acac)_3$ acted as a rhodium precursor [20]. Thus, the synthesis method proposed in this work for 0.01–0.5% Rh/g-C_3N_4 photocatalysts can be considered quite promising, especially considering the acceptable activity at low mass fractions of the metal.

Supplementary Materials: The following supporting information can be downloaded at: https://www.mdpi.com/article/10.3390/nano13152176/s1, Figure S1. (a,b) HRTEM images of 0.5% Rh/g-C_3N_4 and Fourier transform from the highlighted image. Figure S2. (a,b) HRTEM images of 0.5% Rh/g-C_3N_4 and 0.5% Pd/g-C_3N_4. Figure S3. H_2 evolution rates for photocatalysts 0.5% Pd/g-C_3N_4 and 0.5% Rh/g-C_3N_4 synthesized from different metal precursors. Table S1. Actual metal content in the samples determined with ICP AES. Table S2. Surface element atomic concentration calculated based on XPS data of fresh 0.5% Pd/g-C_3N_4 and 0.5% Rh/g-C_3N_4 photocatalysts and these photocatalysts after cyclic runs in 0.1 M NaOH and water (Figures 8 and 9).

Author Contributions: A.V.Z.: investigation, data curation, visualization and writing—original draft preparation; D.B.V.: investigation, data curation, visualization and writing—original draft preparation; S.N.B.: investigation, data curation and visualization; E.Y.G.: investigation and data curation; A.A.S.: investigation and visualization; S.V.C.: investigation and data curation; E.A.K.: writing—original draft preparation, supervision, conceptualization, funding acquisition and project administration. All authors have read and agreed to the published version of the manuscript.

Funding: This work was funded by the Russian Science Foundation (Grant No. 21-13-00314; https://rscf.ru/en/project/21-13-00314/).

Institutional Review Board Statement: Not applicable.

Informed Consent Statement: Not applicable.

Data Availability Statement: The data presented in this study are available on request from the corresponding author.

Acknowledgments: The XPS and HR TEM experiments were performed using facilities of the shared research center "National center of investigation of catalysts" at Boreskov Institute of Catalysis.

Conflicts of Interest: The authors declare no conflict of interest.

References

1. Krausmann, F.; Schaffartzik, A.; Mayer, A.; Eisenmenger, N.; Gingrich, S.; Haberl, H.; Fischer-kowalski, M. *Social Ecology*; Springer: Berlin/Heidelberg, Germany, 2016. [CrossRef]
2. World Meteorological Organization GHG-Bulletin-15_en. *Wmo Greenh. Gas Bull.* **2019**, *15*. Available online: https://library.wmo.int/index.php?lvl=notice_display&id=21620 (accessed on 23 July 2023).
3. Wang, Z.; Li, C.; Domen, K. Recent Developments in Heterogeneous Photocatalysts for Solar-Driven Overall Water Splitting. *Chem. Soc. Rev.* **2019**, *48*, 2109–2125. [CrossRef] [PubMed]
4. Nagar, R.; Srivastava, S.; Leo, S.; Amaya, S.L.; Tanna, A. Recent Developments in State-of-the-Art Hydrogen Energy Technologies—Review of Hydrogen Storage Materials. *Sol. Compass* **2023**, *5*, 100033. [CrossRef]
5. Hermesmann, M.; Müller, T.E. Green, Turquoise, Blue, or Grey? Environmentally Friendly Hydrogen Production in Transforming Energy Systems. *Prog. Energy Combust. Sci.* **2022**, *90*, 100996. [CrossRef]
6. Crabtree, G.W.; Dresselhaus, M.S.; Buchanan, M.V. The Hydrogen Economy. *Phys. Today* **2004**, *57*, 39–44. [CrossRef]
7. Zou, C.; Li, J.; Zhang, X.; Jin, X.; Xiong, B.; Yu, H.; Liu, X.; Wang, S.; Li, Y.; Zhang, L.; et al. Industrial Status, Technological Progress, Challenges, and Prospects of Hydrogen Energy. *Nat. Gas Ind. B* **2022**, *9*, 427–447. [CrossRef]
8. Kozlova, E.A.; Parmon, V.N. Heterogeneous Semiconductor Photocatalysts for Hydrogen Production from Aqueous Solutions of Electron Donors. *Russ. Chem. Rev.* **2017**, *86*, 870–906. [CrossRef]
9. Lakhera, S.K.; Rajan, A.; Rugma, T.P.; Bernaurdshaw, N. A Review on Particulate Photocatalytic Hydrogen Production System: Progress Made in Achieving High Energy Conversion Efficiency and Key Challenges Ahead. *Renew. Sustain. Energy Rev.* **2021**, *152*, 111694. [CrossRef]
10. Fujishima, A.; Honda, K. Electrochemical Photolysis of Water at a Semiconductor Electrode. *Nature* **1972**, *238*, 37–38. [CrossRef]
11. Şen, Z. Solar Energy in Progress and Future Research Trends. *Prog. Energy Combust. Sci.* **2004**, *30*, 367–416. [CrossRef]
12. Bie, C.; Cheng, B.; Fan, J.; Ho, W.; Yu, J. Enhanced Solar-to-Chemical Energy Conversion of Graphitic Carbon Nitride by Two-Dimensional Cocatalysts. *EnergyChem* **2021**, *3*, 100051. [CrossRef]
13. Li, X.; Shen, R.; Ma, S.; Chen, X.; Xie, J. Graphene-Based Heterojunction Photocatalysts. *Appl. Surf. Sci.* **2018**, *430*, 53–107. [CrossRef]
14. Gupta, A.; Likozar, B.; Jana, R.; Chanu, W.C.; Singh, M.K. A Review of Hydrogen Production Processes by Photocatalytic Water Splitting—From Atomistic Catalysis Design to Optimal Reactor Engineering. *Int. J. Hydrogen Energy* **2022**, *47*, 33282–33307. [CrossRef]
15. Zhurenok, A.V.; Vasilchenko, D.B.; Kozlova, E.A. Comprehensive Review on G-C_3N_4-Based Photocatalysts for the Photocatalytic Hydrogen Production under Visible Light. *Int. J. Mol. Sci.* **2023**, *24*, 346. [CrossRef]
16. Wang, X.; Maeda, K.; Thomas, A.; Takanabe, K.; Xin, G.; Carlsson, J.M.; Domen, K.; Antonietti, M. A Metal-Free Polymeric Photocatalyst for Hydrogen Production from Water under Visible Light. *Nat. Mater.* **2009**, *8*, 76–80. [CrossRef] [PubMed]
17. Feng, W.; Lei, Y.; Wu, X.; Yuan, J.; Chen, J.; Xu, D.; Zhang, X.; Zhang, S.; Liu, P.; Zhang, L.; et al. Tuning the Interfacial Electronic Structure: Via Au Clusters for Boosting Photocatalytic H_2 Evolution. *J. Mater. Chem. A* **2021**, *9*, 1759–1769. [CrossRef]
18. Huang, H.; Zhao, J.; Weng, B.; Lai, F.; Zhang, M.; Hofkens, J.; Roeffaers, M.B.J.; Steele, J.A.; Long, J. Site-Sensitive Selective CO_2 Photoreduction to CO over Gold Nanoparticles. *Angew. Chemie Int. Ed.* **2022**, *61*, e202204563. [CrossRef]
19. Balraj, G.; Gurrapu, R.; Anil Kumar, A.; Sumalatha, V.; Ayodhya, D. Facile Synthesis and Characterization of Noble Metals Decorated G-C_3N_4 (g-C_3N_4/Pt and g-C_3N_4/Pd) Nanocomposites for Efficient Photocatalytic Production of Schiff Bases. *Results Chem.* **2022**, *4*, 100597. [CrossRef]
20. Krishnan, A.; Yoosuf, M.; Archana, K.; Arsha, A.S.; Viswam, A. Metal Derivative (MD)/g-C_3N_4 Association in Hydrogen Production: A Study on the Fascinating Chemistry behind, Current Trend & Future Direction. *J. Energy Chem.* **2023**, *80*, 562–583. [CrossRef]
21. Ding, J.; Sun, X.; Wang, Q.; Li, D.S.; Li, X.; Li, X.; Chen, L.; Zhang, X.; Tian, X.; Ostrikov, K. (Ken) Plasma Synthesis of Pt/g-C_3N_4 Photocatalysts with Enhanced Photocatalytic Hydrogen Generation. *J. Alloys Compd.* **2021**, *873*, 159871. [CrossRef]
22. Trasatti, S. Work Function, Electronegativity, and Electrochemical Behaviour of Metals. III. Electrolytic Hydrogen Evolution in Acid Solutions. *J. Electroanal. Chem.* **1972**, *39*, 163–184. [CrossRef]

23. Ooka, H.; Huang, J.; Exner, K.S. The Sabatier Principle in Electrocatalysis: Basics, Limitations, and Extensions. *Front. Energy Res.* **2021**, *9*, 654460. [CrossRef]
24. Greeley, J.; Jaramillo, T.F.; Bonde, J.; Chorkendorff, I.; Nørskov, J.K. Computational High-Throughput Screening of Electrocatalytic Materials for Hydrogen Evolution. *Nat. Mater.* **2006**, *5*, 909–913. [CrossRef] [PubMed]
25. Quaino, P.; Juarez, F.; Santos, E.; Schmickler, W. Volcano Plots in Hydrogen Electrocatalysis-Uses and Abuses. *Beilstein J. Nanotechnol.* **2014**, *5*, 846–854. [CrossRef] [PubMed]
26. Zhang, Y.; Ligthart, D.A.J.M.; Quek, X.Y.; Gao, L.; Hensen, E.J.M. Influence of Rh Nanoparticle Size and Composition on the Photocatalytic Water Splitting Performance of Rh/Graphitic Carbon Nitride. *Int. J. Hydrogen Energy* **2014**, *39*, 11537–11546. [CrossRef]
27. Li, F.; Xu, B.; You, X.; Gao, G.; Xu, R.; Wang, X.L.; Yao, Y.F. In-Situ Synthesis of Pd Nanocrystals with Exposed Surface-Active Facets on g-C_3N_4 for Photocatalytic Hydrogen Generation. *Int. J. Hydrogen Energy* **2023**, *48*, 12299–12308. [CrossRef]
28. Lu, R.; Hu, M.; Xu, C.; Wang, Y.; Zhang, Y.; Xu, B.; Gao, D.; Bi, J.; Fan, G. Hydrogen Evolution from Hydrolysis of Ammonia Borane Catalyzed by Rh/g-C_3N_4 under Mild Conditions. *Int. J. Hydrogen Energy* **2018**, *43*, 7038–7045. [CrossRef]
29. Peng, Y.; He, Y.; Wang, Y.; Long, Y.; Fan, G. Sustainable One-Pot Construction of Oxygen-Rich Nitrogen-Doped Carbon Nanosheets Stabilized Ultrafine Rh Nanoparticles for Efficient Ammonia Borane Hydrolysis. *J. Colloid Interface Sci.* **2021**, *594*, 131–140. [CrossRef]
30. Li, Y.T.; Zhang, X.L.; Peng, Z.K.; Liu, P.; Zheng, X.C. Highly Efficient Hydrolysis of Ammonia Borane Using Ultrafine Bimetallic RuPd Nanoalloys Encapsulated in Porous G-C_3N_4. *Fuel* **2020**, *277*, 118243. [CrossRef]
31. Wang, M.; Zhang, Y.; Jin, C.; Li, Z.; Chai, T.; Zhu, T. Fabrication of Novel Ternary Heterojunctions of Pd/g-C_3N_4/Bi_2MoO_6 Hollow Microspheres for Enhanced Visible-Light Photocatalytic Performance toward Organic Pollutant Degradation. *Sep. Purif. Technol.* **2019**, *211*, 1–9. [CrossRef]
32. Yin, Z.; Tian, Y.; Gao, P.; Feng, L.; Liu, Y.; Du, Z.; Zhang, L. Photodegradation Mechanism and Genetic Toxicity of Bezafibrate by Pd/g-C_3N_4 Catalysts under Simulated Solar Light Irradiation: The Role of Active Species. *Chem. Eng. J.* **2020**, *379*, 122294. [CrossRef]
33. Liu, G.; Huang, Y.; Lv, H.; Wang, H.; Zeng, Y.; Yuan, M.; Meng, Q.; Wang, C. Confining Single-Atom Pd on g-C_3N_4 with Carbon Vacancies towards Enhanced Photocatalytic NO Conversion. *Appl. Catal. B Environ.* **2021**, *284*, 119683. [CrossRef]
34. Vasilchenko, D.; Topchiyan, P.; Tsygankova, A.; Asanova, T.; Kolesov, B.; Bukhtiyarov, A.; Kurenkova, A.; Kozlova, E. Photoinduced Deposition of Platinum from $(Bu_4N)_2[Pt(NO_3)_6]$ for a Low Pt-Loading Pt/TiO_2Hydrogen Photogeneration Catalyst. *ACS Appl. Mater. Interfaces* **2020**, *12*, 48631–48641. [CrossRef] [PubMed]
35. Vasilchenko, D.; Zhurenok, A.; Saraev, A.; Gerasimov, E.; Cherepanova, S.; Tkachev, S.; Plusnin, P.; Kozlova, E. Highly Efficient Hydrogen Production under Visible Light over G-C_3N_4-Based Photocatalysts with Low Platinum Content. *Chem. Eng. J.* **2022**, *445*, 136721. [CrossRef]
36. Vasilchenko, D.; Zhurenok, A.; Saraev, A.; Gerasimov, E.; Cherepanova, S.; Kovtunova, L.; Tkachev, S.; Kozlova, E. Platinum Deposition onto G-C_3N_4 with Using of Labile Nitratocomplex for Generation of the Highly Active Hydrogen Evolution Photocatalysts. *Int. J. Hydrogen Energy* **2022**, *47*, 11326–11340. [CrossRef]
37. Berdyugin, S.N.; Vasilchenko, D.B.; Baidina, I.A.; Korenev, S.V.; Korolkov, I.V. Crystal Structure and Properties of $[Rh_2(H_2O)_8(\mu\text{-}OH)_2](NO_3)_4{\cdot}4H_2O$. *J. Struct. Chem.* **2018**, *59*, 664–668. [CrossRef]
38. Vasilchenko, D.; Topchiyan, P.; Berdyugin, S.; Plyusnin, P.; Shayapov, V.; Baidina, I.; Komarov, V.; Bukhtiyarov, A.; Gerasimov, E. Tetranitratopalladate(II) Salts with Tetraalkylammonium Cations: Structural Aspects, Reactivity, and Applicability toward Palladium Deposition for Catalytic Applications. *Inorg. Chem.* **2021**, *60*, 2983–2995. [CrossRef]
39. Guo, Y.; Li, J.; Yuan, Y.; Li, L.; Zhang, M.; Zhou, C.; Lin, Z. A Rapid Microwave-Assisted Thermolysis Route to Highly Crystalline Carbon Nitrides for Efficient Hydrogen Generation. *Angew. Chemie* **2016**, *128*, 14913–14917. [CrossRef]
40. Vu, N.; Nguyen, C.; Kaliaguine, S.; Do, T. Synthesis of G-C_3N_4 Nanosheets by Using a Highly Condensed Lamellar Crystalline Melamine–Cyanuric Acid Supramolecular Complex for Enhanced Solar Hydrogen Generation. *ChemSusChem* **2019**, *12*, 291–302. [CrossRef]
41. Liu, H.; Chen, D.; Wang, Z.; Jing, H.; Zhang, R. Microwave-Assisted Molten-Salt Rapid Synthesis of Isotype Triazine-/Heptazine Based g-C_3N_4 Heterojunctions with Highly Enhanced Photocatalytic Hydrogen Evolution Performance. *Appl. Catal. B Environ.* **2017**, *203*, 300–313. [CrossRef]
42. Dong, F.; Zhao, Z.; Xiong, T.; Ni, Z.; Zhang, W.; Sun, Y.; Ho, W.-K. In Situ Construction of G-C_3N_4/g-C_3N_4 Metal-Free Heterojunction for Enhanced Visible-Light Photocatalysis. *ACS Appl. Mater. Interfaces* **2013**, *5*, 11392–11401. [CrossRef] [PubMed]
43. Matveev, A.V.; Kaichev, V.V.; Saraev, A.A.; Gorodetskii, V.V.; Knop-Gericke, A.; Bukhtiyarov, V.I.; Nieuwenhuys, B.E. Oxidation of Propylene over Pd(5 5 1): Temperature Hysteresis Induced by Carbon Deposition and Oxygen Adsorption. *Catal. Today* **2015**, *244*, 29–35. [CrossRef]
44. Wang, M.; Shen, S.; Li, L.; Tang, Z.; Yang, J. Effects of Sacrificial Reagents on Photocatalytic Hydrogen Evolution over Different Photocatalysts. *J. Mater. Sci.* **2017**, *52*, 5155–5164. [CrossRef]
45. Kumaravel, V.; Imam, M.; Badreldin, A.; Chava, R.; Do, J.; Kang, M.; Abdel-Wahab, A. Photocatalytic Hydrogen Production: Role of Sacrificial Reagents on the Activity of Oxide, Carbon, and Sulfide Catalysts. *Catalysts* **2019**, *9*, 276. [CrossRef]

46. Pellegrin, Y.; Odobel, F. Les Donneurs d'électron Sacrificiels Pour La Production de Combustible Solaire. *Comptes Rendus Chim.* **2017**, *20*, 283–295. [CrossRef]
47. Vasilchenko, D.; Tkachenko, P.; Tkachev, S.; Popovetskiy, P.; Komarov, V.; Asanova, T.; Asanov, I.; Filatov, E.; Maximovskiy, E.; Gerasimov, E.; et al. Sulfuric Acid Solutions of $[Pt(OH)_4(H_2O)_2]$: A Platinum Speciation Survey and Hydrated Pt(IV) Oxide Formation for Practical Use. *Inorg. Chem.* **2022**, *61*, 9667–9684. [CrossRef]